Large-Scale Synthesis of Long Crystalline Cu2-xSe Nanowire Bundles by Water-Evaporation-Induced Self-Assembly and Their Application in Gas Sensing

ARTICLE *in* ADVANCED FUNCTIONAL MATERIALS · JUNE 2009

Impact Factor: 11.81 · DOI: 10.1002/adfm.200801430

ADVANCED FUNCTIONAL MATERIALS

Large-Scale Synthesis of Long Crystalline $Cu_{2-x}Se$ Nanowire Bundles by Water-Evaporation-Induced Self-Assembly and Their Application in Gas Sensing

By *Jun Xu, Weixin Zhang,* Zeheng Yang, Shaixia Ding, Chunyan Zeng, Lingling Chen, Qiang Wang,* and *Shihe Yang**

By a facile water evaporation process without adding any directing agent, $Cu_{2-x}Se$ nanowire bundles with diameters of 100–300 nm and lengths up to hundreds of micrometers, which comprise crystalline nanowires with diameters of 5–8 nm, are obtained. Experiments reveal the initial formation/stacking of CuSe nanoplates and the subsequent transformation to the $Cu_{2-x}Se$ nanowire bundles. A water-evaporation-induced self-assembly (WEISA) mechanism is proposed, which highlights the driving force of evaporation in promoting the nanoplate stacking, CuSe-to-$Cu_{2-x}Se$ transformation and the growth/bundling of the $Cu_{2-x}Se$ nanowires. The simplicity, benignancy, scalability, and high-yield of the synthesis of this important nanowire material herald its numerous applications. As one example, the use of the $Cu_{2-x}Se$ nanowire bundles as a photoluminescence-type sensor of humidity is demonstrated, which shows good sensitivity, ideal linearity, quick response/recovery and long lifetime in a very wide humidity range at room temperature.

1. Introduction

Semiconductor nanowires have been extensively studied in recent years because of their fundamental importance and potential applications in fabricating nanoscale electronic, optical, optoelectronic, electrochemical, and electromechanical devices.[1] Substantial efforts have been devoted to the development of new synthetic methodologies for inorganic semiconductor nanowires, which are controllable, flexible, simple, and environmentally friendly.[2] However, current methods for fabricating semiconductor nanowires thinner than 10 nm and longer than 10 μm are still limited. Among the various techniques described in the literature, template-directed synthesis, using the channels contained in mesoporous silica[2a] and reverse micelles,[2b] was successful for obtaining long nanowires with high aspect ratios. Surfactant-assisted solution-phase method has also been developed to synthesize semiconductor nanowires with diameters less than 10 nm.[3] However, the lengths of the nanowires prepared so far were generally limited to less than a few micrometers.

Copper selenides ($Cu_{2-x}Se$) exist in different stoichiometric forms. Their complex structures and valence states result in some unique optical and electrical properties. Copper selenides are well-known p-type semiconductors having potential applications in solar cells, optical filters, nanoswitches, thermoelectric and photoelectric transformers, and superconductors.[4] Many recent efforts have been devoted to the synthesis of copper selenides micro- and nanocrystallites with various morphologies,[5] such as particles,[5a] tubes,[5b,5c] cages,[5d] and flake-like structures.[5e] There have been a few reports on the synthesis of copper selenide nanowires. For example, $Cu_{2-x}Se$ nanowires with lengths of several micrometers and diameters of 30–50 nm have been prepared by employing selenium-bridged copper cluster $[Cu_4\{Se_2P(O^iPr)_2\}_4]$ as precursor in a chemical vapor deposition (CVD) process.[6a] Also prepared are arrays of copper selenide nanowires of mixed compositions of Cu_3Se_2/$Cu_{2-x}Se$ or $Cu_{2-x}Se$/Cu in various proportions with lengths of several micrometers and diameters of 13–17 nm by using porous anodic aluminum oxide film as template.[6b] However, to our knowledge, there has been no report on facile solution synthesis of thin copper selenide nanowires with lengths up to 10 μm.

Herein, we report on the successful synthesis of thin and long crystalline copper selenide ($Cu_{2-x}Se$) nanowires in large-scale via a simple approach—water evaporation induced self-assembly (WEISA). This is achieved simply by evaporating the $Cu(NO_3)_2$ and alkaline selenium aqueous solution, without using any surfactant and template. The thin $Cu_{2-x}Se$ nanowires with diameters of 5–8 nm are held together in bundles with uniform diameters of 100–300 nm and lengths up to hundreds of

[*] Prof. W. Zhang, J. Xu, Prof. Z. Yang, Dr. S. Ding, C. Zeng, L. Chen, Q. Wang
Anhui Key Laboratory of Controllable Chemical Reaction & Material Chemical Engineering
School of Chemical Engineering
Hefei University of Technology
Hefei, Anhui 230009, P.R. China
E-mail: wxzhang@hfut.edu.cn
Prof. S. Yang
Department of Chemistry
The Hong Kong University of Science and Technology
Clear Water Bay, Kowloon, Hong Kong
E-mail: chsyang@ust.hk

DOI: 10.1002/adfm.200801430

micrometers. Among the outstanding features of our method are its simplicity, scalability, and effectiveness. To demonstrate potential utilities of the interesting $Cu_{2-x}Se$ nanowire bundles, we have further investigated their photoluminescence sensitivity to humidity. Experimental results indicate that the novel sensor exhibits good sensitivity, ideal linearity, quick response/recovery, and long lifetime in a very wide humidity range at room temperature.

2. Results and Discussion

2.1. Morphologies and Structures

The as-prepared product is first characterized by X-ray powder diffraction (XRD) analysis and field-emission scanning electron microscopy (FESEM). Figure 1a shows the XRD pattern of the product prepared at 140 °C for 5 h. All the diffraction peaks can be well indexed to cubic $Cu_{2-x}Se$ with lattice constant $a = 5.728$ Å, which is consistent with the value ($a = 5.739$ Å) given in the standard card (JCPDF 06-0680). Figure 1b and c show typical FESEM images of a large quantity of one-dimensional nanostructures (nanowire bundles) with lengths up to hundreds of micrometers and diameters of 100–300 nm. High-magnification FESEM image in Figure 1d clearly reveals that the bundles are further constructed from many thin nanowires. It is remarkable from Figure 1 that the product is solely composed of $Cu_{2-x}Se$ nanowire bundles without obvious impurities, and all of the nanowires are orientationally aligned and grow uniformly along the bundle.

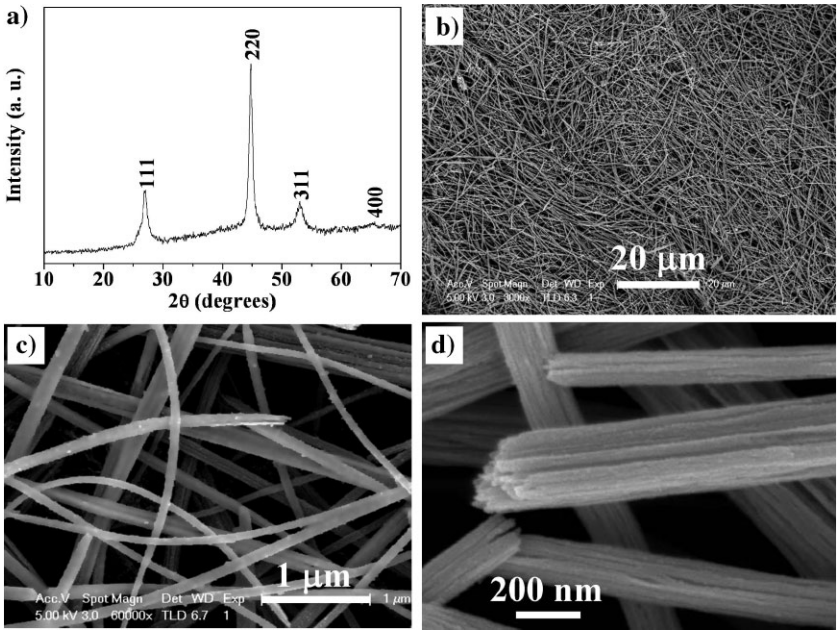

Figure 1. a) XRD pattern of the $Cu_{2-x}Se$ nanowire bundles prepared in a beaker in a fan-forced oven after reaction at 140 °C for 5 h. b–d) FESEM images of the $Cu_{2-x}Se$ nanowire bundles: b,c) low magnification; d) high magnification.

The morphology and structure of the $Cu_{2-x}Se$ product is further investigated by transmission electron microscopy (TEM), high-resolution transmission electron microscopy (HRTEM) and selected-area electron diffraction (SAED) pattern. The low magnification TEM image of the long $Cu_{2-x}Se$ nanowire bundles in Figure 2a indicates that each bundle has a uniform diameter. TEM image at higher magnification (Fig. 2b) clearly reveals that all the nanowire bundles are made up of many thin nanowires, which are well aligned along their longitudinal direction. On the basis of the SAED pattern recorded from a single bundle (inserted in Fig. 2a), the well-defined spots clearly indicate the oriented alignment of the constituent $Cu_{2-x}Se$ nanowires in the bundle along [110]. Note that the (220) and $(\bar{2}\bar{2}0)$ dots are actually ellipsoidal in shape elongated perpendicular to the nanowire axis, implying the thinness and/or small mis-alignment of the nanowires in the bundle.[7]

More structural details are provided by HRTEM studies. The HRTEM image of a nanowire bundle shown in Figure 3a clearly shows that the constituent nanowires have diameters of only 5–8 nm and there exist distinct boundaries between the nanowires. Energy-dispersive X-ray spectroscopy (EDX) of the nanowires (Fig. S1 of the Supporting Information) suggests that the nanowire bundles only consist of elements of copper and selenium. The enlarged details of the nanowires in the white frame of Figure 3a are shown in Figure 3b and c. The lattice fringe with a constant spacing of 0.20 nm (Fig. 3b) matches well with the spacing between the (220) planes of $Cu_{2-x}Se$, and also supports the nanowire growth direction of [110]. On the other hand, the fringe spacing of 0.35 nm (Fig. 3c) corresponds to the $3 \times (2\bar{2}4)$ lattice spacing of the cubic $Cu_{2-x}Se$ crystal. It is seen that the $[1\bar{1}2]$ direction makes almost a right angle with the nanowire axis, in concurrence with the theoretical angle (90 °) subtending the [110] and $[1\bar{1}2]$ axes of the cubic $Cu_{2-x}Se$. The corresponding SAED pattern of the single $Cu_{2-x}Se$ nanowire in Figure 3b in the $[\bar{1}11]$ zone axis is shown in Figure 3d, which further indicates its single crystalline face centered cubic (fcc) structure. We believe that a stacking fault lying parallel to the $(\bar{1}11)$ plane may be responsible for the occurrence of $\frac{1}{3}\{2\bar{2}4\}$ forbidden reflections in the $[\bar{1}11]$ SAED pattern and the corresponding $3 \times (2\bar{2}4)$ superlattice fringe in the $[\bar{1}11]$ HRTEM image (Fig. 3c). Similarly, $\frac{1}{3}\{422\}$ forbidden reflections in the [111] SAED patterns were observed previously in Ag, Au, and Si nanocrystals with the common fcc crystal structure,[8] and well elaborated by Wang's group.[8h]

2.2. Growth of the $Cu_{2-x}Se$ Nanowires as a Function of Reaction Time

To understand the formation mechanism of the long $Cu_{2-x}Se$ nanowire bundles assembled from oriented thin nanowires, we tracked the time course of nanowire growth process, revealing that the nanowire bundles were

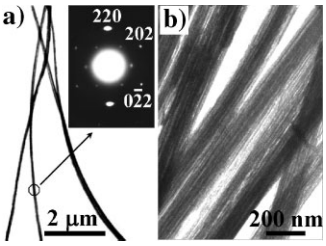

Figure 2. TEM images of the $Cu_{2-x}Se$ nanowire bundles: a) lower magnification; b) higher magnification. Inset in (a) is the corresponding SAED pattern of a single nanowire bundle.

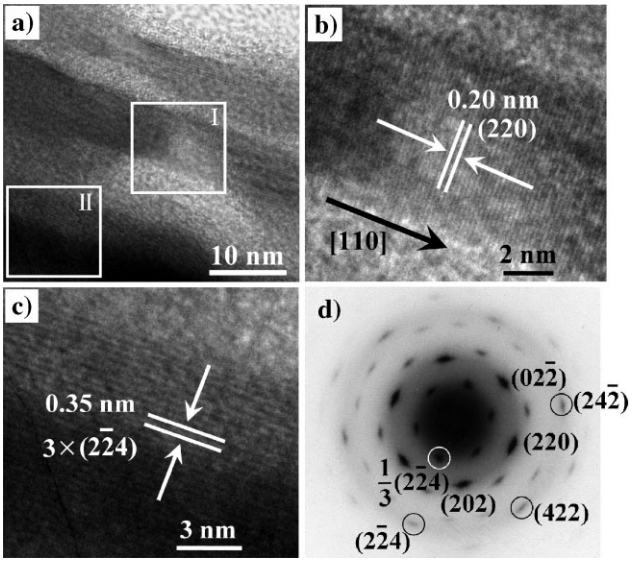

Figure 3. a) HRTEM image of $Cu_{2-x}Se$ nanowire bundles; b) HRTEM image of a single $Cu_{2-x}Se$ nanowire indicated with the white frame I in Figure 3a; c) HRTEM image of the $Cu_{2-x}Se$ nanowire indicated with the white frame II in Figure 3a; d) SAED pattern of the $Cu_{2-x}Se$ nanowire shown in Figure 3b.

formed by WEISA coupled with a dissolution/crystallization process.

The XRD patterns of the samples at different reaction stages are shown in Figure 4. Figure 4a is the XRD pattern of the product obtained shortly after adding the $Cu(NO_3)_2$ solution into the hot alkaline selenium solution (83 °C). All the diffraction peaks can be well indexed to hexagonal CuSe (JCPDF 34-0171). When the mixture in the beaker is kept in fan-forced oven at 140 °C for 40 min, the XRD pattern of the product is still indexed to hexagonal CuSe as shown in Figure 4b. Figure 4c shows the XRD pattern of the product obtained after evaporating the mixture at 140 °C for 90 min (at this stage, there still exists some liquid in the mixture), indicating that the intermediate product is a mixture of hexagonal CuSe and cubic $Cu_{2-x}Se$. The diffraction peaks marked with * come from $Cu_{2-x}Se$ (JCPDF 06-0680). At last, as shown in Figure 4d, single phase of $Cu_{2-x}Se$ is obtained after heating for 5 h.

Accordingly, the final product forming reactions may take place as follows in three stages.

i) Preparation of the alkaline selenium aqueous solution

$$3\,Se + 6\,NaOH \rightarrow 2\,Na_2Se + Na_2SeO_3 + 3\,H_2O \quad (1)$$

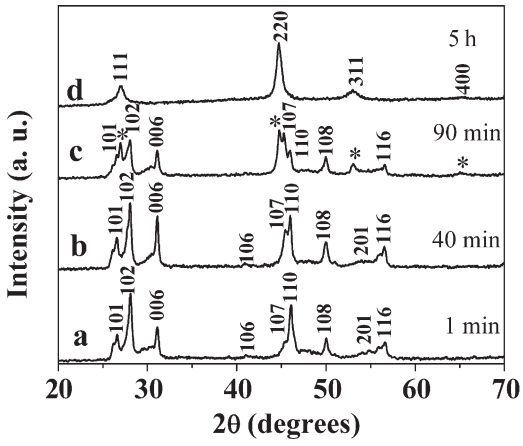

Figure 4. XRD patterns of the CuSe products prepared after different reaction time: a) 1 min; b) 40 min; c) 90 min; and d) 5 h.

ii) Precipitation of CuSe (when the $Cu(NO_3)_2$ solution was added to the alkaline selenium aqueous solution, CuSe was formed immediately).

$$Cu^{2+} + Se^{2-} \rightarrow CuSe \quad (2)$$

iii) Transformation from CuSe to $Cu_{2-x}Se$ (after the solution in the beaker was kept in the fan-forced oven at 140 °C for ~60 min, CuSe began to change gradually into $Cu_{2-x}Se$).

$$(2-x)\,CuSe \rightarrow Cu_{2-x}Se + (1-x)\,Se \quad (3)$$

From the K_{sp} values of CuSe (7.94×10^{-49}) and Cu_2Se (1.58×10^{-61}), we can calculate the necessary concentration of copper ions needed to form CuSe and Cu_2Se precipitates according to the following equations, respectively.

$$[Cu^{2+}] = \frac{K_{sp}(CuSe)}{[Se^{2-}]},\ [Cu^{+}] = \sqrt{\frac{K_{sp}(Cu_2Se)}{[Se^{2-}]}} \quad (4)$$

In the solution, if $[Se^{2-}] = 1$ M, for the formation of CuSe, the required $[Cu^{2+}] = 7.94 \times 10^{-49}$ M, and for the formation of Cu_2Se, the required $[Cu^{+}] = 3.97 \times 10^{-32}$ M. It is obvious that CuSe is easier to precipitate than Cu_2Se and will do so first from the solution under the condition of our experiment.

On the other hand, the formation of cubic $Cu_{2-x}Se$ is considered to result from the redox reaction between CuSe and Se^{2-} anions. The calculated emf ($E^\circ = 0.933$ V) of this reaction is positive based on the half-cell potentials (E° (Cu^{2+}/Cu^{+}) = +0.153 V, E° (Se/Se^{2-}) = −0.78 V), which implies that there is a spontaneous tendency for the formation of $Cu_{2-x}Se$ phase. With the increase of reaction time and the evaporation of H_2O solvent, the concentration of the superfluous Se^{2-} anions increases as well as the temperature of the system arising from the boiling point increase. All these conditions should facilitate the liquid–solid phase redox reaction between CuSe and Se^{2-}

ions. The Cu^{2+} ions dissolved and diffused from the solid CuSe react with Se^{2-} ions from the solution at the solid–liquid interface via a redox process, resulting in the formation of $Cu_{2-x}Se$ phase;[5a] here the x value was determined to be 0.37 from the XPS results shown in Table S1.

FESEM and TEM were employed to further investigate the formation mechanism of the $Cu_{2-x}Se$ nanowire bundles. Six samples collected after different reaction time were examined. In the first stage, when the $Cu(NO_3)_2$ solution was added to the alkaline selenium solution, CuSe nanoparticles with a size of 15–25 nm were formed immediately as shown in Figure S2a. After being heated for 40 min, the CuSe nanoparticles in the solution have grown into hexagonal nanoplates. It can be seen from the SEM image in Figure 5a that these hexagonal CuSe nanoplates have a size of 100–400 nm. A TEM image of the CuSe nanoplates is given in Figure S2b. The corresponding SAED pattern (inset of Fig. S2b of the Supporting Information) of a single nanoplate along the [001] zone axis indicates that it is a single crystal. For a longer reaction time (60 min), the tendency of some nanoplates to stack together to form 1D nanostructures of a $CuSe/Cu_{2-x}Se$ mixture is clearly observed in the FESEM image shown in Figure 5b. And the tendency of the nanoplates to split has also been observed in the TEM image shown in Figure S2c. Shown in Figure 5c and d are FESEM images of the sample after evaporation for 90 min, which reveals the formation of longitudinally stacked bundles from the self-assembly of small split CuSe nanoplates. At this stage, as shown in Equation (3), the Cu^{2+} ions dissolved and diffused from the CuSe nanoplates react with Se^{2-} anions from the solution at the liquid–solid interface to form $Cu_{2-x}Se$ nuclei. Consequently, the continuous dissolution–diffusion of Cu^{2+} ions from the CuSe nanoplates results in the splitting of CuSe nanoplates to many small nanoplates (Fig. S2d of the Supporting Information). Moreover, the formation of these small nanoplates increases the contact surface of CuSe with Se^{2-} ions and further facilitates the dissolution/splitting of the CuSe nanoplates. This process can be viewed as a chemical etching process of CuSe nanoplates by Se^{2-} anions from the solution in a redox reaction. At the same time, the produced $Cu_{2-x}Se$ nuclei grew into nanorods along [110] direction. With the prolongation of reaction time, these split CuSe nanoplates were further etched, and converted to form fine $Cu_{2-x}Se$ nanorods. When the reaction time was extended to 3.5 h, $Cu_{2-x}Se$ nanowire bundles were eventually formed from the laterally split but longitudinally joined nanoplates via an oriented growth process.[9] Both the FESEM image (Fig. 5e) and TEM image (Fig. S2e of the Supporting Information) reveal that no CuSe nanoplates can be obviously observed at this stage. At last, when the solvent H_2O was completely evaporated after heat treatment for 5 h, large scale of $Cu_{2-x}Se$ nanowire bundles with diameters of 100–300 nm and lengths up to hundreds of micrometers, which comprise well-aligned crystalline nanowires with diameters of 5–8 nm, were obtained as shown in Figure 5f and Figure S2f of the Supporting Information.

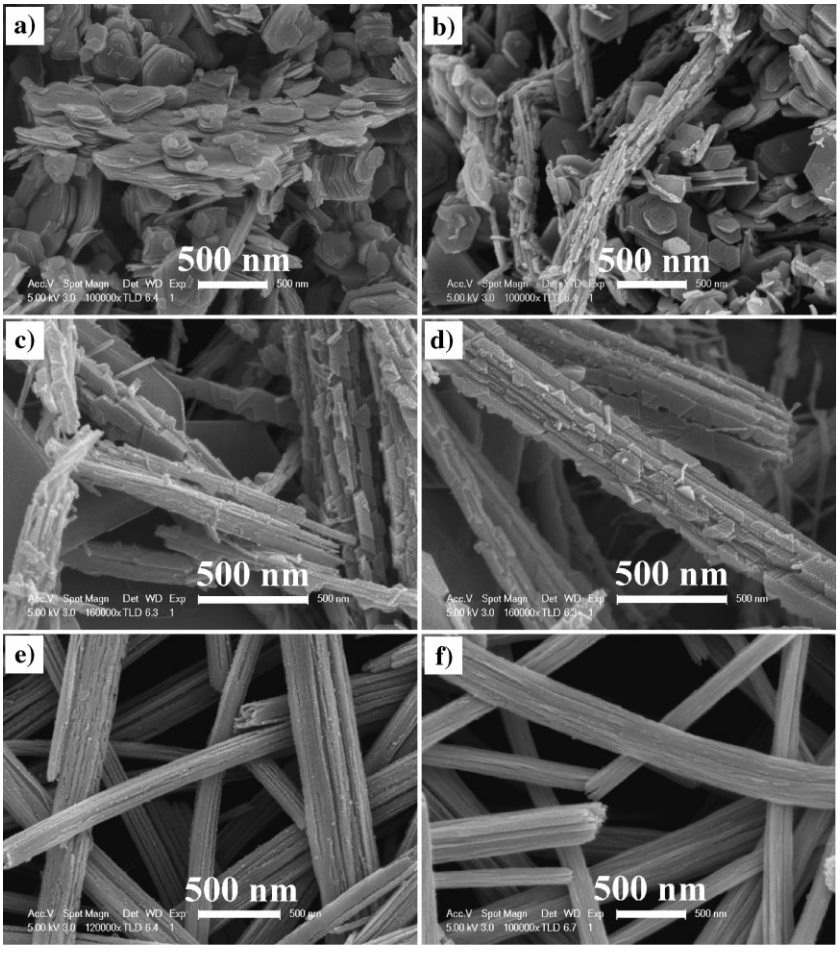

Figure 5. FESEM images of the CuSe products formed after different reaction times: a) 40 min; b) 60 min; c,d) 90 min; e) 3.5 h; and f) 5 h.

On the basis of the experimental results, a possible mechanism for the formation process of the $Cu_{2-x}Se$ nanowire bundles by evaporation of solvent is displayed in Scheme 1. Here, water evaporation is considered to play an important role in the formation of the long $Cu_{2-x}Se$ nanowire bundles in at least three aspects: i) it induces the self-assembly of the CuSe nanoplates to form 1D bundles; ii) it helps the dissolution/splitting of CuSe nanoplates and the subsequent formation of $Cu_{2-x}Se$ nanorods in the bundles; iii) it contributes to the oriented growth of longitudinally joined $Cu_{2-x}Se$ nanorods in the bundles to form the $Cu_{2-x}Se$ nanowire bundles. To our knowledge, this interesting transformation of CuSe nanoplates into long $Cu_{2-x}Se$ nanowire bundles arising from evaporation-induced self-assembly coupled with dissolution/crystallization have not been observed previously. Of course, many of details about the formation mechanism have yet to be worked out in future experiments.

Although growth of inorganic nanowire bundles has been reported previously,[10] the

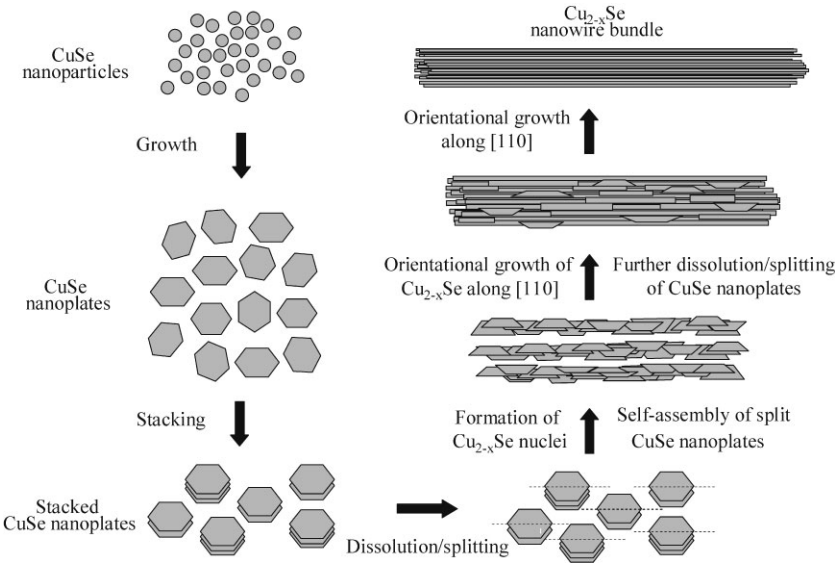

Scheme 1. Schematic representation of the process involved in the formation of $Cu_{2-x}Se$ nanowire bundles by the water evaporation method.

lengths of the bundles obtained were limited to only a few micrometers in most cases. One prominent feature of our $Cu_{2-x}Se$ nanowire bundles is the lengths up to hundreds of micrometer, which results from the controllable solvent evaporation induced self-assembly. During the evaporation process, solvent flow caused by H_2O evaporation helps to transfer the sediment of CuSe nanoplates and results in the longitudinally self-assembly of the CuSe nanoplates. Meanwhile, the long-range interactive force, induced by the surface tension of the solvent and the attractive interaction between the nanoplates may contribute to the stacking of CuSe nanoplates as well as the self-assembly of the CuSe nanoplates into bundle structures. Obviously, the longitudinally self-assembly of the CuSe nanoplates is prerequisite for the formation of the long $Cu_{2-x}Se$ nanowire bundles. On the other hand, the continuous evaporation of the solvent H_2O concentrates the solution and increases the temperature of the system, which is beneficial to the phase transformation from CuSe to $Cu_{2-x}Se$.

A control experiment without solvent evaporation was carried out under otherwise identical conditions. The CuSe product obtained in a Teflon-lined stainless steel autoclave of 50 mL capacity at 140 °C for 5 h exists only as flakes and short nanorods (Fig. S3 of the Supporting Information). This result further proves that the solvent evaporation indeed induces and enhances the assembly of the nanostructures to the final nanowire bundles.

Another prominent feature of our product is that the $Cu_{2-x}Se$ nanowire bundles are assembled from many thin nanowires with diameters less than 10 nm, due to the unique dissolution/splitting of the stacked CuSe nanoplates and the subsequent oriented growth of $Cu_{2-x}Se$ along [110] direction.

2.3. Humidity Sensing Properties

As we know, one of the goals for developing novel nanostructured materials is to put them to better use in advanced devices. During the past few decades, research efforts have been mainly devoted to resistor-type gas sensors of semiconducting metal oxides,[11] such as ZnO,[11a] SnO_2,[11b] SiO_2,[11c] In_2O_3,[11d] Co_3O_4,[11e] V_2O_5,[11f] CuO,[11g] and Cu_2O.[11h] Studies of photoluminescence-type gas sensing materials are mostly focused on porous silicon[12] and organic dyes.[13] Applications of metal chalcogenide semiconductors for photoluminescence-type gas sensors have not been reported previously. As an important p-type semiconductor, $Cu_{2-x}Se$ is considered to have great potential in luminescence gas sensors. Considering that the $Cu_{2-x}Se$ nanowire bundles with hierarchical nanostructures might exhibit good gas sensing performance, we set out to measure the humidity sensing characteristics of photoluminescence (PL) due to the wide-spread demand for humidity monitoring.[14]

Shown in Figure 6 are photoluminescence (PL) spectra of the long $Cu_{2-x}Se$ nanowire bundles measured on a fluorescence spectrophotometer using a Xe lamp at an excitation wavelength of 370 nm, under different relative humidity. The relative humidity was controlled by tuning the flow rate of pure nitrogen and nitrogen saturated with water vapor at 18 °C. In each of the curves, a strong emission peak centered at 450 nm corresponding to the energy band gap of 2.76 eV can be observed. The peak shows obvious blue-shift relative to that of $Cu_{2-x}Se$ nanowires with diameters of 30–50 nm reported previously,[6a] due probably to the size effects of the thin nanowires. Most importantly, the PL intensity of the $Cu_{2-x}Se$ nanowire bundles at 450 nm increases with the relative humidity (RH). For example, the PL intensity of the $Cu_{2-x}Se$ nanowire bundles under 65% RH (the nitrogen saturated with water vapor at 18 °C) is around 3400, which is significantly higher than that (2625) under exposure to pure nitrogen (0% RH).

Figure 7 shows the PL responses of the $Cu_{2-x}Se$ nanowire bundle sensor as the surrounding gas was switched between 65%

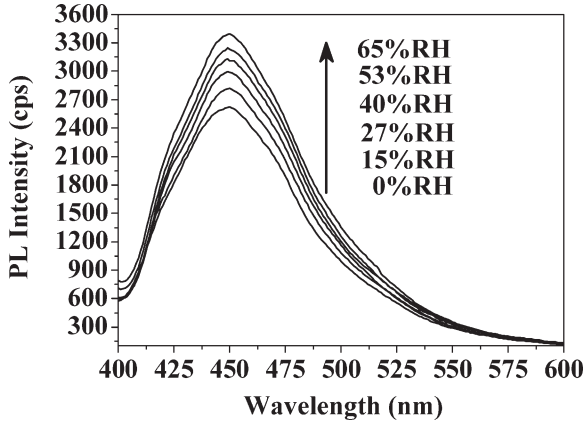

Figure 6. PL spectra of the $Cu_{2-x}Se$ nanowire bundles exposed to different RH at 18 °C.

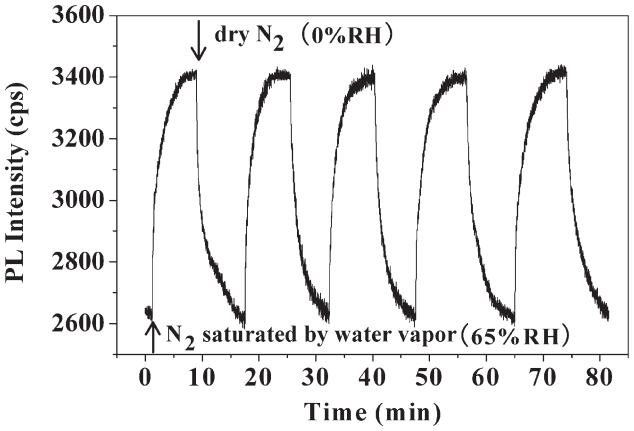

Figure 7. PL intensity profile of the $Cu_{2-x}Se$ nanowire bundle sensor as the surrounding gas was switched between 65% and 0% RH, with the excitation and emission wavelengths set at 370 and 450 nm, respectively.

and 0% RH. The response and recovery times, defined as corresponding to 95% and 5% of the maximum PL intensity, are about 5.9 and 6.3 min, respectively. One can see that the PL intensity changes are fully reversible in a period of a few hours we have studied.

The PL intensity response of the $Cu_{2-x}Se$ nanowire bundle sensor to different RH is characterized and shown in Figure 8a. It can be seen that the nanowire bundle sensor can operate in a broad range of RH (0–65% RH); the response and recovery time at different RH maintains the same; and the PL intensity is enhanced regularly with the increase of RH at 18 °C. Figure 8b plots the PL intensity versus the RH at 18 °C. Clearly, there is a linear relationship between the PL intensity and RH of the sensed gas. The correlation coefficient of the plots, R, is estimated to be 0.99706 by the least squares method. This result indicates that the $Cu_{2-x}Se$ nanowire bundle sensor shows excellent linearity. As we know, many of the reported humidity sensor is not good for humidity detection below 65% RH.[15] However, our $Cu_{2-x}Se$ nanowire bundle sensor shows a very linear response in a broad relative humidity range, which holds great potential for accurate detection of low humidity. Notice that our measurement system has not been optimized and the results are still preliminary, and the $Cu_{2-x}Se$ nanowire bundle sensor certainly has much room for improvement.

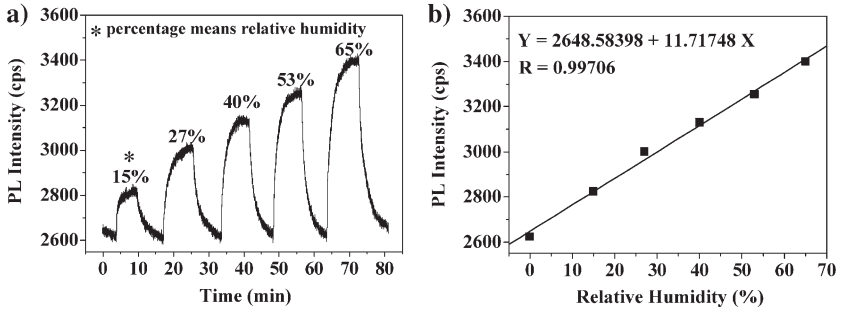

Figure 8. a) PL intensity profile of the $Cu_{2-x}Se$ nanowire bundle sensor as a function of RH at 18 °C, with excitation and emission wavelengths being at 370 and 450 nm, respectively. b) The linear relationship between PL intensity and RH.

In gas sensors, the changed PL intensity are related to both physical properties of the analytes such as dipole moment/dielectric constant, and equilibrium concentrations of the analytes inside nanostructured materials.[12a] In our case, the enhancement of PL intensity of the $Cu_{2-x}Se$ nanowire bundles exposed to nitrogen containing water vapor can be explained by an electron transfer mechanism as follows. $Cu_{2-x}Se$ is a p-type semiconductor, hence holes are the main carriers. Thus gas molecules can act as electron donors to $Cu_{2-x}Se$. Photo-excited $Cu_{2-x}Se$ nanowires promote the formation of excitons. When the $Cu_{2-x}Se$ nanowire bundle sensor is exposed to nitrogen containing water vapor instead of pure nitrogen, oxygen atoms from the dipolar H_2O molecules shall be preferentially absorbed on the surface of $Cu_{2-x}Se$ by donating their lone-pair electrons. The increased amount of valence electrons in $Cu_{2-x}Se$ attracts the holes, thus reduces the tendency of nonradiative transitions, and consequently results in the PL intensity enhancement.

In order to check the possible impact of the O_2 from air to our measurements, we carried out a control experiment by using dry air to substitute the N_2 flow as carrier gas. Figure S4 of the Supporting Information shows the PL responses of the $Cu_{2-x}Se$ nanowire bundles switched between 65% and 0% RH by N_2 and dry air, respectively. In Figure S4a of the Supporting Information, dry air was used as the carrier gas in the first five cycles and N_2 was used as the carrier gas in the last five cycles. In Figure S4b of the Supporting Information, N_2 was used as the carrier gas in the first five cycles and dry air was used as the carrier gas in the last five cycles. By comparing Figure S4a and b of the Supporting Information, it can be found that the $Cu_{2-x}Se$ nanowire bundle sensor exhibits almost the same sensing properties in air as in N_2. In addition, the PL intensity response of the $Cu_{2-x}Se$ nanowire bundle sensor to different RH by using dry air as carrier gas was also characterized and the result is shown in Figure S5a of the Supporting Information. Excellent linear relationship between the PL intensity and RH of the sensed gas can be seen in Figure S5b of the Supporting Information.

The results presented above reveal that the presence of oxygen has no obvious influence on the sensing performance of the $Cu_{2-x}Se$ nanowire bundles. This can be explained from two aspects. On one hand, the O_2 from air as an oxidizing gas does not affect the stability of $Cu_{2-x}Se$ nanowire bundles. On the other hand, oxygen molecules as well as nitrogen molecules are nonpolar molecules (the dipolar moment of oxygen molecule is 0 D), which we believe contribute little to donate their lone-pair electrons. However, water has two very polar covalent bonds between oxygen and hydrogen. Because the water molecule is bent (its oxygen atom is sp^3 hybridized), the two bond dipole moments add up to give water a relatively large molecular dipolar moment (1.861D). Oxygen atoms from the dipolar H_2O molecules shall be preferentially absorbed on the surface of $Cu_{2-x}Se$ by donating their lone-pair electrons, and resulting in the sharp increase of PL intensity. The result from the comparison experiment with dry air as carrier gas further confirms the mechanism of the PL intensity enhancement by water molecules. Furthermore, it indicates that the $Cu_{2-x}Se$

nanowire bundle sensor can be aptly used in ambient air environment.

The kinetics and equilibrium of the above adsorption and desorption process are expected to be very sensitive to the surface environments. The $Cu_{2-x}Se$ nanowire bundle sample has a BET surface area of 25.7580 $m^2 g^{-1}$ due to its large surface-to-volume ratio, which is much larger than that of bulk $Cu_{2-x}Se$ (2.3723 $m^2 g^{-1}$) (Fig. S6 of the Supporting Information). The comparison test shows that the sensitivity of this bulk $Cu_{2-x}Se$ sensor to humidity is much lower than that of the $Cu_{2-x}Se$ nanowire bundle sensor, although it exhibits faster response and recovery (Fig. S7 of the Supporting Information). The faster response and recovery of the bulk $Cu_{2-x}Se$ sensor is considered to result from the small surface area of the bulk $Cu_{2-x}Se$, which facilitates the fast absorption and desorption of water molecules.

3. Conclusions

In summary, large-scale crystalline $Cu_{2-x}Se$ nanowire bundles with lengths up to hundreds of micrometers and diameters of 100–300 nm have been successfully synthesized by an evaporation-induced self-assembly method. These nanowire bundles are in actuality assembled from many thin $Cu_{2-x}Se$ nanowires with diameters of 5–8 nm. Mechanistic studies show that the formation process of $Cu_{2-x}Se$ nanowire bundles by water evaporation is distinct from the previously reported synthesis of 1D nanomaterials. The results reveal that the self-assembly process clearly contributes to the creation of the long bundles, while the dissolution/splitting of CuSe nanoplates is confirmed to be the prerequisite for the synthesis of these thin nanowires. The PL intensity response of the $Cu_{2-x}Se$ nanowire bundles to humidity has been investigated at room temperature. The excellent linearity in sensitivity, along with the fast response and recovery, long lifetime, and no need for heat regeneration of the sensor has been demonstrated. The present work establishes a roadmap for the controlled synthesis of $Cu_{2-x}Se$ nanowire bundles by using the simple and scalable WEISA method and opens up a new avenue for the fabrication of photoluminescence-type gas sensors of semiconductor nanomaterials. Potentially, the methodologies reported here can be extended to the synthesis of other 1D semiconductor materials and the sensing of different gases.

4. Experimental

Synthesis of $Cu_{2-x}Se$ Nanowire Bundles: A typical procedure was as follows: 0.15 g of Se powder, 5.0 g of NaOH and 20 mL of distilled water were put in a 125 mL beaker with heating and stirring. After the Se powder was dissolved at ~83 °C, an alkaline selenium aqueous solution (deep red) was prepared and then 1.5 mL of $Cu(NO_3)_2$ aqueous solution (0.5 M) was added in it. Then the beaker was kept in fan-forced oven at 140 °C for 5 h. As time passed, water, as the solvent in the solution, was gradually evaporated and became less and less and finally the dry products deposited on the bottom of the beaker. The product was collected and washed with hot distilled water and ethanol for several times. Then the product was dried in air at 60 °C.

Characterization: The as-prepared samples were characterized by XRD in a Rigaku D/max-γ B X-ray diffractometer with a Cu Kα radiation source ($\lambda = 1.5418$ Å) operated at 40 kV and 80 mA. FESEM measurement was taken by JEOL-7500B scanning electron microscope. TEM images and HRTEM images were taken with Hitachi H-800 and JEOL-2010 transmission electron microscope performed at an accelerating voltage of 200 kV, respectively. Surface areas of the samples were determined by BET measurements on nitrogen adsorption at 77 K with a Beckman Coulter Surface Area Analyzer SA 3100.

Humidity Sensor Measurements: All measurements of photoluminescence (PL) response were performed in an adapted photoluminescence setup. Relative humidity response was tested using a setup composing of a gas flow control system, a colorimetric ware and a Hitachi F-4500 fluorescence spectrophotometer at room temperature (18 °C; as shown in Fig. S8 of the Supporting Information: $\lambda_{ex} = 370$ nm, Ex slit = 2.5 nm, Em slit = 5 nm). The humidity sensor was fabricated by affixing the thin pressed pellet (13×10 mm^2) of $Cu_{2-x}Se$ nanowire bundles on a hard black paper substrate (14×40 mm^2), which was put in the colorimetric ware operating with nitrogen as a carrier gas for PL measurements. Measurements of concentration dependence of sensor response were performed by introducing controlled amounts of water vapor in nitrogen into the system. After stabilization of photoluminescence intensity analyte was subsequently blown off by purging the system with pure nitrogen. Relative humidity was controlled by adjusting the flow rate of the nitrogen through the two gas flow controllers. The total flow rate was maintained at 1000 mL min^{-1}. The relative humidity was calibrated by a commercial humidity meter. Dry air was also used to substitute the N_2 flow as a carrier gas.

Acknowledgements

This project has been financially supported by the National Natural Science Foundation of China (NSFC Grants 20871038, 20876031 and 20576024) and the Educational Department of Anhui Provincial Government (TD200702). S. Y. acknowledges support from the Research Grant Council of Hong Kong (GRF 604206). Supporting Information is available online from Wiley InterScience or from the authors.

Received: September 26, 2008
Revised: November 12, 2008
Published online: April 8, 2009

[1] a) Y. Qin, X. D. Wang, Z. L. Wang, *Nature* **2008**, *451*, 809. b) Z. L. Wang, *Adv. Mater.* **2000**, *12*, 1295. c) S. Frank, P. Poncharal, Z. L. Wang, W. A. de Heer, *Science* **1998**, *280*, 1744. d) X. Duan, Y. Huang, Y. Cui, J. Wang, C. M. Lieber, *Nature* **2001**, *409*, 66. e) Y. Cui, Q. Wei, H. Park, C. M. Lieber, *Science* **2001**, *293*, 1289. f) D. S. Wang, C. H. Hao, W. Zheng, Q. Peng, T. H. Wang, Z. M. Liao, D. P. Yu, Y. D. Li, *Adv. Mater.* **2008**, *20*, 2628. g) Y. W. Tan, X. Y. Xue, Q. Peng, H. Zhao, T. H. Wang, Y. D. Li, *Nano Lett.* **2007**, *7*, 3723.

[2] a) N. Coombs, D. Khushalani, S. Oliver, G. A. Ozin, G. C. Shen, I. Sokolov, H. Yang, *J. Chem. Soc, Dalton Trans.* **1997**, 3941. b) H. Shi, L. Qi, J. Ma, H. Cheng, *Chem. Commun.* **2002**, 1704. c) B. H. Hong, S. C. Bae, C. W. Lee, S. Jeong, K. S. Kim, *Science* **2001**, *294*, 348. d) J. D. Holmes, K. P. Johnston, R. C. Doty, B. A. Korgel, *Science* **2000**, *287*, 1471. e) J. J. Urban, W. S. Yun, Q. Gu, H. Park, *J. Am. Chem. Soc.* **2002**, *124*, 1186. f) Y. Bondo, K. Takayanagi, *Science* **2000**, *289*, 606.

[3] a) Y. W. Jun, S. M. Lee, N. J. Kang, J. Cheon, *J. Am. Chem. Soc.* **2001**, *123*, 5150. b) Y. W. Jun, Y. Y. Jung, J. Cheon, *J. Am. Chem. Soc.* **2002**, *124*, 615. c) F. Dumestre, B. Chaudret, C. Amiens, M. Fromen, M. Casanove, P. Renaud, P. Zurcher, *Angew. Chem. Int. Ed.* **2002**, *41*, 4286. d) F. Dumestre, B. Chaudret, C. Amiens, M. Respaud, P. Fejes, P. Renaud, P. Zurcher, *Angew. Chem. Int. Ed.* **2003**, *42*, 5213. e) C. Qian, F. Kim, L. Ma, F. Tsui, P. D. Yang, J. Liu, *J. Am. Chem. Soc.* **2004**, *126*, 1195. f) J. W. Grebinski, K. L. Hull, J. Zhang, T. H. Kosel, M. Kuno, *Chem. Mater.* **2004**, *16*, 5260.

[4] a) V. M. Bhuse, P. P. Hankare, K. M. Garadkar, A. S. Khomane, *Mater. Chem. Phys.* **2003**, *80*, 82. b) C. Lévy-Clément, M. Neumann-Spallart, S. K. Haram, K. S. V. Santhanam, *Thin Solid Films* **1997**, *302*, 12. c) A. M. Hermann, L. Fabick, *J. Cryst. Growth* **1983**, *61*, 658.

[5] a) W. X. Zhang, X. M. Zhang, L. Zhang, J. X. Wu, Z. H. Hui, Y. W. Cheng, J. W. Liu, Y. Xie, Y. T. Qian, *Inorg. Chem.* **2000**, *39*, 1838. b) J. Xu, W. X. Zhang, Z. H. Yang, S. H. Yang, *Inorg. Chem.* **2008**, *47*, 699. c) Y. Jiang, Y. Wu, B. Xie, S. Y. Zhang, Y. T. Qian, *Nanotechnology* **2004**, *15*, 283. d) H. L. Cao, X. F. Qian, J. T. Zai, J. Yin, Z. K. Zhu, *Chem. Commun.* **2006**, 4548. e) Y. Xie, X. W. Zheng, X. C. Jiang, J. Lu, L. Y. Zhu, *Inorg. Chem.* **2002**, *41*, 387.

[6] a) Y. J. Hsu, C. M. Hung, Y. F. Lin, B. J. Liaw, T. S. Lobana, S. Y. Lu, C. W. Liu, *Chem. Mater.* **2006**, *18*, 3323. b) A. Jagminas, R. Juškėnas, I. Gailiutė, G. Statkutė, R. Tomašiunas, *J. Cryst. Growth* **2006**, *294*, 343.

[7] Z. P. Liu, D. Xu, J. B. Liang, J. M. Shen, S. Y. Zhang, Y. T. Qian, *J. Phys. Chem. B* **2005**, *109*, 10699.

[8] a) A. I. Kirkland, D. A. Jefferson, D. G. Duff, P. P. Edwards, I. Gameson, B. F. G. Johnson, D. J. Smith, *Proc. R. Soc. London A* **1993**, *440*, 589. b) R. Jin, Y. W. Cao, C. A. Mirkin, K. L. Kelly, G. C. Schatz, J. G. Zheng, *Science* **2001**, *294*, 1901. c) D. Cherns, *Philos. Mag.* **1974**, *30*, 549. d) A. I. Kirkland, D. A. Jefferson, D. G. Duff, P. P. Edwards, *Inst. Phys. Conf. Ser.* **1989**, *98*, 375. e) N. Tanaka, J. M. Cowley, *Mater. Res. Soc. Symp. Proc.* **1985**, *41*, 155. f) J. C. Heyraud, J. J. Métois, *Surf. Sci.* **1980**, *100*, 519. g) A. H. Carim, K. K. Lew, J. M. Redwing, *Adv. Mater.* **2001**, *13*, 1489. h) V. Germain, J. Li, D. Ingert, Z. L. Wang, M. P. Pileni, *J. Phys. Chem. B* **2003**, *107*, 8717.

[9] a) H. G. Yang, H. C. Zeng, *Angew. Chem. Int. Ed.* **2004**, *43*, 5930. b) Y. Chang, H. C. Zeng, *Cryst. Growth Des.* **2004**, *4*, 397. c) B. Liu, S. H. Yu, L. J. Li, Q. Zhang, F. Zhang, K. Jiang, *Angew. Chem. Int. Ed.* **2004**, *43*, 4745.

[10] a) D. F. Moore, Y. Ding, Z. L. Wang, *J. Am. Chem. Soc.* **2004**, *126*, 14372. b) J. Zhang, S. Y. Wei, J. Lin, J. J. Luo, S. J. Liu, H. S. Song, E. Elawad, X. X. Ding, J. M. Gao, S. R. Qi, C. C. Tang, *J. Phys. Chem. B* **2006**, *110*, 21680.

[11] a) Y. F. Qiu, S. H. Yang, *Adv. Funct. Mater.* **2007**, *17*, 1345. b) Y. L. Wang, X. C. Jiang, Y. N. Xia, *J. Am. Chem. Soc.* **2003**, *125*, 16176. c) B. H. King, A. Gramada, J. R. Link, M. J. Sailor, *Adv. Mater.* **2007**, *19*, 4044. d) N. Du, H. Zhang, B. D. Chen, X. Y. Ma, Z. H. Liu, J. B. Wu, D. R. Yang, *Adv. Mater.* **2007**, *19*, 1641. e) W. Y. Li, L. N. Xu, J. Chen, *Adv. Funct. Mater.* **2005**, *15*, 851. f) J. F. Liu, X. Wang, Q. Peng, Y. D. Li, *Adv. Mater.* **2005**, *17*, 764. g) J. T. Zhang, J. F. Liu, Q. Peng, X. Wang, Y. D. Li, *Chem. Mater.* **2006**, *18*, 867. h) H. G. Zhang, Q. S. Zhu, Y. Zhang, Y. Wang, L. Zhao, B. Yu, *Adv. Funct. Mater.* **2007**, *17*, 2766.

[12] a) J. Dian, T. Chvojka, V. Vrkoslav, I. Jelínek, *Phys. Stat. Sol.* **2005**, *2*, 3481. b) T. Chvojka, V. Vrkoslav, I. Jelínek, J. Jindřich, M. Lorenc, J. Dian, *Sens. Actuators B* **2004**, *100*, 246. c) W. J. Salcedo, F. J. R. Fernandez, J. C. Rubim, *Spectrochim. Acta Part A* **2004**, *60*, 1065. d) B. H. Han, I. Manners, M. A. Winnik, *Chem. Mater.* **2005**, *17*, 3160.

[13] a) Z. Wang, A. R. McWilliams, C. E. B. Evans, X. Lu, S. Chung, M. A. Winnik, I. Manner, *Adv. Funct. Mater.* **2002**, *12*, 415. b) Z. Q. Zhou, R. Shinar, A. J. Allison, J. Shinar, *Adv. Funct. Mater.* **2007**, *17*, 3530. c) J. Kunzelman, B. R. Crenshaw, C. Weder, *J. Mater. Chem.* **2007**, *17*, 2989. d) N. Nakamura, Y. Amao, *Sens. Actuators B* **2003**, *92*, 98.

[14] a) Z. M. Rittersma, *Sens. Actuators A* **2002**, *96*, 196. b) C. Lee, G. Lee, *Sensor Lett.* **2005**, *3*, 1. c) Z. Chen, C. Lu, *Sensor Lett.* **2005**, *3*, 274.

[15] a) H. L. Tai, Y. D. Jiang, G. Z. Xie, J. S. Yu, X. Chen, *Sens. Actuators B* **2007**, *125*, 644. b) X. F. Zhou, J. Zhang, T. Jiang, X. H. Wang, Z. Q. Zhu, *Sens. Actuators A* **2007**, *135*, 209. c) D. Patil, Y.-K. Seo, Y. K. Hwang, J.-S. Chang, P. Patil, *Sens. Actuators B* **2008**, *128*, 374. d) M. L. Singla, S. Awasthi, A. Srivastava, *Sens. Actuators B* **2007**, *127*, 580. e) K. P. Biju, M. K. Jain, *Thin Solid Films* **2008**, *516*, 2175. f) M.-S. Park, T.-H. Lim, Y.-M. Jeon, J.-G. Kim, S.-W. Joo, M.-S. Gong, *Sens. Actuators B* **2008**, *133*, 166. g) A. Vijayan, M. Fuke, R. Hawaldar, M. Kulkarni, D. Amalnerkar, R. C. Aiyer, *Sens. Actuators B* **2008**, *129*, 106.